Pergamon

0734-743X(95)00026-7

Int. J. Impact Engng Vol. 18, No. 1, pp. 1–22, 1996

0734-743X/96 $9.50+0.00

SCALE MODEL EXPERIMENTS WITH CERAMIC LAMINATE TARGETS

CHARLES E. ANDERSON, JR†, SCOTT A. MULLIN†, ANDREW J. PIEKUTOWSKI‡, NEIL W. BLAYLOCK† and KEVIN L. POORMON‡

†Southwest Research Institute, Materials and Structures Division, P.O. Drawer 28510, San Antonio, TX 78228-0510, U.S.A. and ‡University of Dayton Research Institute, Impact Physics Laboratory, 300 College Park, Dayton, OH 45469-0182, U.S.A.

(*Received* 15 *February* 1994; *in revised form* 16 *March* 1995)

Summary—Ballistic impact experiments were performed on ceramic laminate targets at three scale sizes, nominally 1/3, 1/6, and 1/12, to quantify the effects of scale on various responses, in particular, the ballistic limit velocity. The experiments were carefully designed and controlled so that the different scale sizes were high fidelity replicas of each other. A variety of responses, such as residual projectile quantities, hole size, and the extent of bulging, were measured. Some of the measured quantities showed little or no dependence on scale size, whereas other quantities, particularly the ballistic limit velocity, were found to vary with scale size. The percentage difference was quantified, and the results extrapolated to estimate full-scale response from the subscale tests.

NOTATION

a	regression parameter in Eqn (1)
B	height (extent) of bulging of the rear target surface
C	height of crater front
D	projectile diameter
D_i	interior damage diameter
E_c	critical energy per unit area
H	entrance hole (crater) diameter
H_{min}	minimum entrance hole diameter
H_{max}	maximum entrance hole diameter
L	initial projectile length
L_r	residual projectile length
p	regression parameter in Eqn (1)
P	depth of penetration
P_{exp}	experimentally measured depth of penetration
$P_{degrade}$	degraded penetration due to impact yaw
P_∞	penetration into a semi-infinite target
T	target thickness
V	impact velocity
V_{BL}	ballistic limit velocity
V_r	residual velocity
V_s	striking (impact) velocity
ΔP_r	penetration needed to reach original rear surface of target
ΔP_∞	increment of penetration in a semi-infinite target
ΔV	increment in velocity required for increment in penetration
γ	impact inclination (total yaw)
γ_{cr}	critical yaw angle
λ	scale size

1. INTRODUCTION

Scale models are commonly used in experimental investigations. At ordnance velocities, scaled projectiles and targets are generally used to limit the cost of experiments. In addition, since gun systems are kinetic-energy limited, smaller projectile masses must be used to obtain impact velocities greater than 2.0 km/s. However, there has been a reluctance on the part of many applied researchers to accept scale model data in lieu of full-scale data for actual

projectile–target interactions. This reluctance is generally attributable to a belief that full-scale performance cannot be predicted accurately from subscale data. Unfortunately, documentation to either support or refute this belief is essentially nonexistent.

Important parameters, such as geometry, material properties, and impact conditions, can be formed into nondimensional terms, referred to as Pi terms; for example, see Ref. [1]. According to the principles of similitude modeling, when Pi terms (those relating geometry, material characteristics, and initial conditions) are kept invariant between two different experiments, the experiments will display "similar" response. In other words, the values of the response Pi terms will be equal between the experiments. The most common approach to satisfy the requirements imposed by the Pi terms is to develop a replica model. A replica model is one in which the same materials are used in the model as the prototype— within the context of this article, "prototype" refers to the full-scale test articles and experiment—with the only difference being geometric size. The model is constructed so as to mimic the arrangement of the prototype, with corresponding materials at corresponding locations. Such a model is said to be homologous to the prototype. The size of a replica model relative to the prototype is described by the geometric scale factor, denoted by λ. For example, the λ in this work will represent subscale sizes between 1/12 and 1/3. One feature of replica scaling is that velocity is invariant; i.e. for ballistic impact testing, model and prototype projectiles are fired at the same velocity. However, the concept of a replica model contains some inherent issues that may lead to distortions in the subscale model and limit its ability to reproduce full-scale results. In a replica model, the model law results in conflicting requirements on the Pi terms involving strain rate and fracture toughness, thereby making it impossible to keep Pi terms involving these parameters invariant (see Ref. [1] for a more detailed discussion).

Scaling has been the focus of a number of low velocity impact studies ($V \sim 5 - 100$ m/s) of structural impact and dynamic wedge cutting of thin plates; these studies are summarized in Wen and Jones [2]. Depending upon the specifics of the experiments, deviations from geometrical scaling laws have been observed, particularly where there is fracture and tearing. Atkins [3] has addressed the problem of deviations from geometric scaling by using rigid–plastic fracture mechanics and partitioning the total kinetic energy between plastic work and the energy required for creating new fracture surfaces. Since plastic work scales as λ^3, and the fracture energy scales as λ^2, the total energy absorbed scales as λ^x, $2 \leqslant x \leqslant 3$; thus, the deviation from geometric (λ^3) scaling depends upon the amount of energy in fracturing relative to plastic work. This issue will be addressed further at the end of the paper.

Recent work [1, 4, 5], including the present effort, has focused specifically on issues related to scaling of ballistic penetration ($V > 1$ km/s). In these studies, attention has been paid to materials, fabrication, experimental procedures, and terms that distort as scale size changes.

Magness and Leonard performed a series of impact experiments in which tungsten alloy (WA) and depleted uranium (DU) projectiles were fired into rolled homogeneous armor (RHA) [4]. The length-to-diameter (L/D) aspect ratio for the projectiles used in their study was 10. They measured the depths of penetration for semi-infinite targets and the ballistic limit velocities for finite-thickness targets at three scale sizes. Scale factors of 1/3, 1/4, and 1/6 were used. In all cases, there was a trend of improved penetrator performance as the scale size of the experiment increased. In other words, the 1/3-scale targets were more easily penetrated than the 1/6-scale targets. They found increases of up to 6–7% in normalized depths of penetration (P/L) and decreases of 6–7% in ballistic limit velocities over a factor of 2 increase in model size for both the WA and DU penetrators. In these experiments, however, the lateral dimensions of the targets remained the same for all tests. Therefore, the relative proximity of lateral free surfaces was different at each scale. There was concern that this may have been responsible for the apparent scale dependency of the tests, so they repeated a subset of the ballistic limit experiments. The scale dependency decreased, but they still found a 3–4% decrease in the ballistic limit velocity for a factor of 2 increase in model size. Similar results can be inferred from the data in Ref. [5] for WA, $L/D = 20$, projectiles into armor steel targets.

In the present study, the targets were ceramic laminates. Approximately 36% of the thickness of the target was ceramic; the remainder was armor steel. Ballistic tests were conducted at three scale sizes with two targets of different thicknesses. The test methodology

Table 1. Nominal projectile dimensions and masses

Scale size	Diameter (cm)	Length (cm)	Mass (g)
1/3.15	0.8063	16.12	158.9
1/6.30	0.4032	8.064	19.82
1/12.60	0.2016	4.032	2.433

was designed to permit the determination of the ballistic limit velocities. Additionally, a variety of other measurements was performed: hole diameters and crater height on the impact side of the target, bulge height on the exit side, penetration depth for targets not perforated, and residual projectile length and velocity for targets perforated. The overall objective was to determine the magnitude of the scale effect (if any).

2. EXPERIMENTS

2.1. *Projectiles*

Full scale was defined in terms of a long-rod tungsten alloy penetrator with a hemispherical nose, length-to-diameter ratio of 20, and a diameter of 2.54 cm. This was called the prototype projectile for the purpose of defining the subscale projectiles; no full-scale tests were conducted. Subscale projectiles were designed to replicate the prototype at three scale sizes: 1/3.15, 1/6.30, and 1/12.60. The tungsten alloy used for the tests, WN008FH manufactured by GTE (90% tungsten, 8% nickle, and 2% iron), has a density of 17.19 g/cm^3. It was swaged and aged to give an ultimate tensile strength of 1.3 GPa with a nominal elongation of 8% at failure. Its hardness, measured using the Rockwell C scale, was R_c43. Dimensions for the projectiles are listed in Table 1. There is a factor of four between the smallest and largest of the subscale projectiles.

Impact velocities in excess of 2.0 km/s were desired, and launch stresses mandated the use of a puller sabot; otherwise, the projectile would bend or buckle during launch. The use of a puller sabot required that the tungsten rod be grooved or threaded. Since grooves are practical only in mass production (where the sabots can be cast or molded as opposed to machined), the projectiles were threaded over a portion of their length. The size and number of threads depend upon the stress levels during launch and the length of projectile supported by the sabot. Sabot size generally increases as the length of projectile supported increases, so there is a trade-off in sabot mass vs the length of projectile supported by the sabot.† A compromise was necessary in the thread design for the different scales because the threads could not be scaled exactly (using readily available tap and dies); thus, it was decided that the weight percentage in the threads would be held constant. Therefore, the length of the threaded portion was distorted. The threads increased the weight of the rods by approximately 12% relative to the weight had the rods been smooth. (The inner diameter of the threads was the same as the projectile diameter, i.e. the threads were superior to the cylindrical projectile.)

2.2. *Targets*

A schematic of the target is shown in Fig. 1. Thickness proportions of the steel/ceramic/steel layers were selected as 3 : 4 : 4. The target is analogous to a range target used for testing and evaluation; however, to avoid certain proprietary issues, the targets used in this study were not replicas of the range target. *All* components of the targets were sized for geometric

†A small drag cone was placed on the ends of the projectiles. Historically, this has been done on the assumption that this procedure helps the stability of the rods in flight (although the experiments are performed in a rarified atmosphere). Although a puller sabot was used, a metal pusher disc was placed between the obturator and the tail end of the projectile to protect the drag cone during launch.

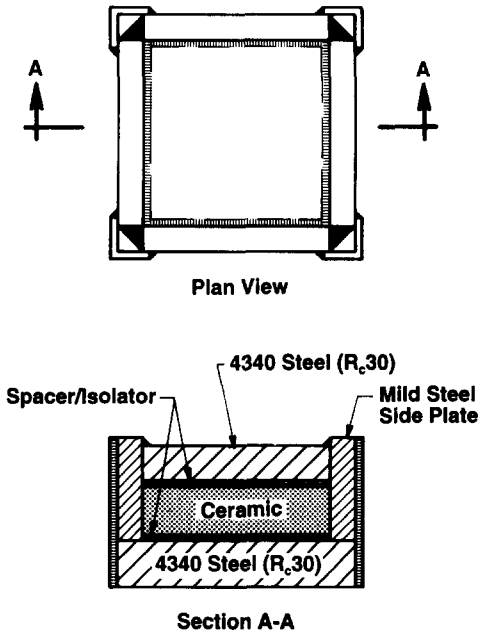

Fig. 1. Schematic of target configuration.

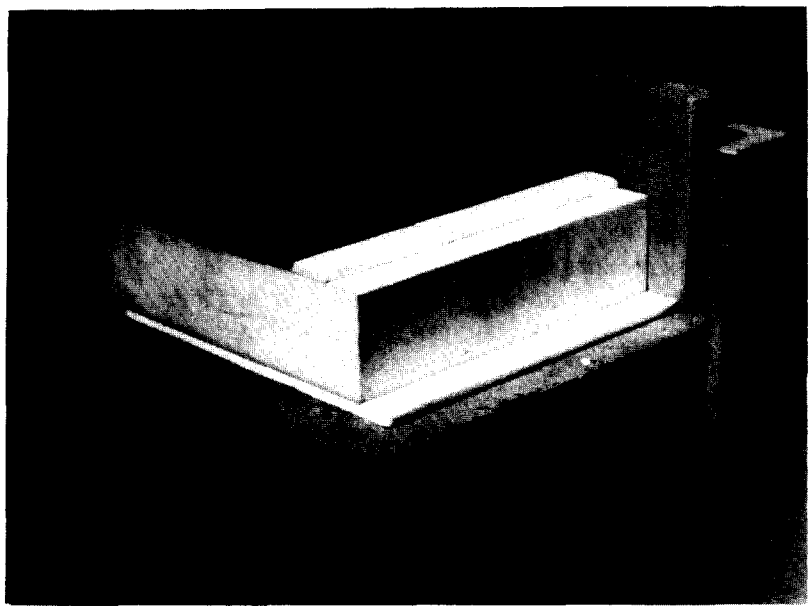

Fig. 2. Photograph of target layup.

scaling between the three scale sizes. The steel was 4340 steel, hardened to $R_c30 \pm 2$; the ceramic was 99.5% pure aluminum oxide manufactured by Ceredyne. Fiberfrax, a non-asbestos, cloth-like (glass) insulating material (density of 0.1 g/cm^3) manufactured by Carborundum, was used to isolate the ceramic tiles from the front and back 4340-steel plates. Weld lines are depicted in Fig. 1 by the closely spaced hash lines or by the heavy black fill. Figure 2 is a photograph of the target showing the various layers, mild steel side plates, and angle iron. Before welding, metal components were preheated to 400°C for a minimum of 3 h; this preheating was necessary to insure integral welds with the 4340 steel. The completed assembly was placed in a 290°C oven for 2–2.5 h. It was then removed from the oven,

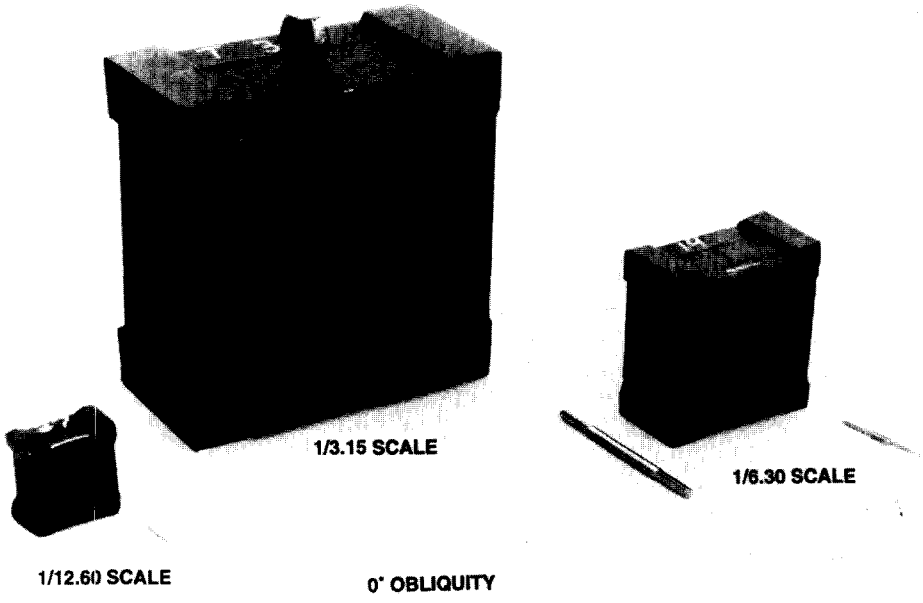

Fig. 3. Photograph of assembled targets.

Table 2. Dimensions for ceramic laminate targets

	1/3.15	1/6.30	1/12.60	1/3.15	1/6.30	1/12.60
	Target 1 thicknesses (cm)			Target 2 thicknesses (cm)		
Front plate: 4340 steel	3.810	1.905	0.953	5.715	2.858	1.429
Layer 2: Fiberfrax	0.635	0.318	0.159	0.635	0.318	0.159
Ceramic: 99.5% Al_2O_3	5.080	2.540	1.270	7.620	3.810	1.905
Layer 4: Fiberfrax	0.635	0.318	0.159	0.635	0.318	0.159
Base plate: 4340 steel	5.080	2.540	1.270	7.620	3.810	1.905
Side plates: mild steel	2.540	1.270	0.635	2.540	1.270	0.635
Angle iron: steel	5.1 × 5.1 × 0.95	2.5 × 2.5 × 0.64	1.3 × 1.3 × 0.32	5.1 × 5.1 × 0.95	2.5 × 2.5 × 0.64	1.3 × 1.3 × 0.32

wrapped in 5.0-cm thick insulating material, and allowed to cool to ambient temperatures. Magnaflux tests were conducted on the targets. These tests showed no cracks or flaws. Figure 3 shows the targets and projectiles at the three different scale sizes.†

Two target sets were designed; the elements in the second target set were 50% thicker than the elements in the first target set. Table 2 provides the dimensions of the various elements in the two target sets.

2.3. *Experimental data*

Projectiles were launched from a two-stage light-gas gun. The two smaller projectiles were launched from a 50/20-mm system; a 75/30-mm system was used for the larger projectile.

†Because of the total weight, a steel lifting eye was added to the 1/3.15-scale target to expedite moving and positioning the target.

Table 3. Experimental data

Test No.	λ	T/L	V_s (km/s)	γ (deg)	V_r/V_s	L_r/D	P/L	B/D	C/D	H_{min}/D	H_{max}/D	D_i/D
8-0084	1/3.15	1.378	2.19	1.50	0.000	0.00	1.40††	1.248††	0.99	2.29	2.29	6.92
8-0085	1/3.15	1.378	2.33	0.79	0.000	0.00	1.33	0.687	1.03	2.40	2.40	9.43
8-0086	1/3.15	1.378	2.33	0.79	0.000	0.00	1.36	0.769	1.04	2.37	2.37	9.43
8-0087	1/3.15	1.378	2.19	2.70	0.000	0.00	1.15	0.086	1.00	2.17	2.17	9.43
8-0088	1/3.15	0.945	2.18	2.12	0.867	4.16	Perf	1.471	0.86	2.07	2.07	+
8-0089	1/3.15	0.945	1.92	2.00	0.766	2.90	Perf	0.945	0.94	1.85	1.85	+
8-0090	1/3.15	0.945	1.67	0.79	0.683	2.65	Perf	1.530	0.72	1.81	1.81	+
8-0091	1/3.15	0.945	1.49	1.50	0.000	0.00	0.72	0.000	0.70	1.70	1.70	5.66
8-0092	1/3.15	0.945	1.56	0.56	0.000	0.00	0.97	1.213	0.67	1.70	1.70	5.97
8-0093	1/3.15	0.945	1.58	6.52	0.000	0.00	<0.63†	0.000	**	**	**	5.50
8-0094	1/3.15	0.945	1.64	0.50	0.433	1.64	Perf	1.522	0.73	1.77	1.77	+
8-0096	1/3.15	0.945	1.61	0.35	0.106	+	Perf	1.405	0.72	1.73	1.73	+
4-1486	1/6.30	0.945	2.16	6.75	0.588	frag	Perf	1.746	**	**	**	+
4-1487	1/6.30	0.945	1.87	1.52	0.861	3.91	Perf	1.763	**	**	**	+
4-1488	1/6.30	0.945	1.63	3.53	0.000	0.00	0.88	0.491	**	**	**	5.97
4-1489	1/6.30	0.945	1.73	3.02	0.572	1.70	Perf	1.992	**	**	**	+
4-1490	1/6.30	0.945	2.19	2.91	0.868	4.35	Perf	1.443	**	**	**	+
4-1491	1/6.30	0.945	1.82	2.55	0.544	0.94	Perf	1.719	**	**	**	+
4-1492	1/6.30	0.945	1.69	0.75	0.000	0.00	0.85	0.295	**	**	**	6.29
4-1493	1/6.30	0.945	1.73	0.56	0.225	1.13	Perf	1.853	**	**	**	+
4-1500	1/6.30	1.378	2.54	8.25	0.000	0.00	1.00	0.000	0.96	2.55	4.62	11.38
4-1501	1/6.30	1.378	2.54	3.29	0.000	0.00	1.31	0.303	1.04	2.38	2.83	10.00
4-1502	1/6.30	1.378	2.68	0.75	0.537	0.50	Perf	1.587	1.13	**	**	+
4-1503	1/6.30	1.378	2.67	5.52	*	*	Perf	1.391	1.07	2.41	**	+
4-1504	1/6.30	1.378	2.63	1.68	0.567	0.76	Perf	1.607	1.11	2.58	2.58	+
4-1505	1/6.30	1.378	2.62	6.91	0.000	0.00	0.19	0.000	**	**	**	9.43
4-1506	1/6.30	1.378	2.62	1.25	0.214	frag	Perf	1.915	**	**	**	+
4-1507	1/6.30	1.378	2.60	1.03	0.469	0.76	Perf	1.739	1.22	2.57	2.57	+
4-1494	1/12.6	0.945	2.14	8.30	0.000	0.00	0.84	0.402	1.21	2.14	4.15	7.54
4-1536	1/12.6	0.945	2.21	8.37	0.000	0.00	0.86	0.402	**	**	**	7.23
4-1537	1/12.6	0.945	2.46	7.19	0.610	frag	Perf	2.037	**	**	**	+
4-1538	1/12.6	0.945	2.30	11.86	0.000	0.00	0.85	0.264	**	**	**	8.05
4-1539	1/12.6	0.945	2.30	5.12	0.739	1.26	Perf	1.836	**	1.89	3.02	+
4-1540	1/12.6	0.945	2.18	0.79	0.358	frag	Perf	1.836	**	**	**	+
4-1541	1/12.6	0.945	2.04	4.99	0.480	1.26	Perf	+	**	**	**	+
4-1542	1/12.6	1.378	2.39	2.02	0.000	0.00	1.26	0.201	**	**	**	8.17
4-1543	1/12.6	1.378	2.60	6.97	0.000	0.00	1.09	0.000	**	**	**	9.68
4-1544	1/12.6	1.378	2.69	13.64	0.000	0.00	0.96	0.000	**	**	**	12.70
4-1545	1/12.6	1.378	2.72	3.58	0.272	frag	Perf	1.924	**	**	**	+
4-1546	1/12.6	1.378	2.76	7.44	0.000	0.00	1.04	0.000	**	**	**	11.44
4-1547	1/12.6	1.378	2.76	14.10	0.000	0.00	<0.91†	0.000	1.38	2.89	5.43	11.57
4-1548	1/12.6	1.378	2.72	13.81	0.000	0.00	<0.91†	0.000	1.63	2.77	6.35	12.45

+ data not available
*X-rays flashed too soon
**pusher hit target, obscuring results
†penetration stopped in ceramic before last steel plate, measurement assumes ceramic was fully penetrated
††integrity of target was compromised before testing.

Velocities were determined using a laser "break" beam system. Projectile yaw and pitch were obtained by orthogonal flash X-rays prior to impact, and combined to give the total impact inclination γ. Table 3 provides the test number, scale size, normalized target thickness (T/L), and total projectile inclination at impact for the 42 tests conducted. Two pairs of orthogonal X-ray heads were used to determine the residual velocity and residual length of the projectile if it perforated the target; these values are also given in Table 3.

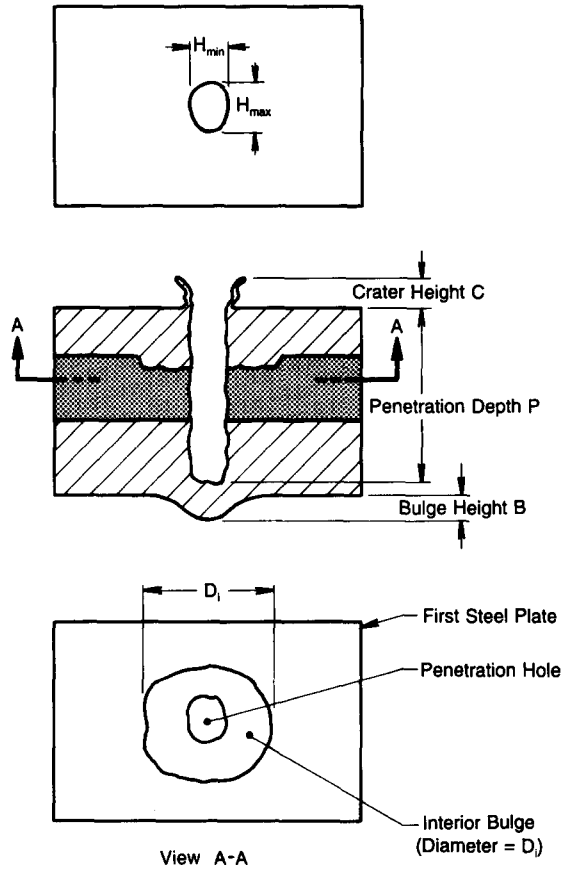

Fig. 4(a). Post-test measurements and notation.

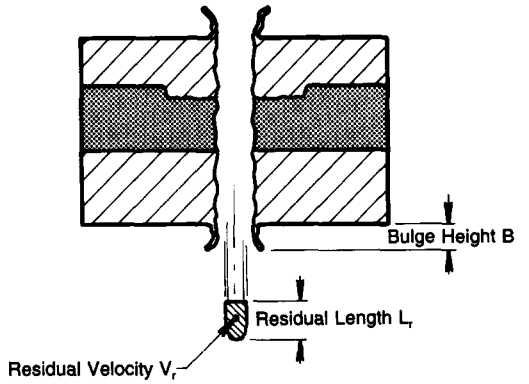

Fig. 4(b). Post-test measurements and notation—perforated target.

The primary objective of the test series was to determine the ballistic limit velocity V_{BL} for each target thickness and scale size. Additionally, parameters were measured so that the effect of scale on other target responses could be determined. Post-test measurements included crater diameter, the extent of bulging on the back side of the target, and the depth of penetration for targets not perforated. Figure 4 provides a schematic of various items measured. Figure 4(a) depicts the nomenclature for a target that was not perforated, and Fig. 4(b) depicts the nomenclature for a perforated target. Target response data, in non-dimensional form, are summarized in Table 3.

As will be seen, the 1/12.6-scale tests were plagued by excessive projectile yaw. This was largely attributed to the mass of the sabot with respect to the projectile mass since any

Table 4. Uncertainty values for the ballistic response measurements (refer to Fig. 4)

Quantity	V_s (km/s)	Yaw (deg)	V_r (km/s)	L_r (mm)	P (mm)	B (mm)	C (mm)	H (mm)	D_i (mm)
Uncertainty	0.01	0.25	0.025	0.5	0.5	0.1	0.1	0.25	2.

asymmetry in the opening of the sabot would be sufficient to perturb the flight of the projectile. Although projectile yaw confounds data analysis, attempts were made to account explicitly for the effects of yaw in some of the analysis.

3. DATA ANALYSIS

3.1. *Measurement uncertainty*

Each of the experimental variables contains some uncertainty in their respective measurements. A concern was that differences in scale might be masked by uncertainty and scatter of the individual measurements. Table 4 lists the uncertainties in measured parameters based upon known accuracies of the measurement devices; repeat measurements, where appropriate, of the same quantity; and variations, where applicable, between minimum and maximum values. The variation in some of the parameters is larger than the precision of the measurements, which for the post-test measurements was approximately 0.02 mm. The residual velocity measurements have a larger uncertainty than the impact velocity measurements only because the residual projectile sometimes tumbled, making it more difficult to determine the exact location of a reference point. As described in the following sections, measurement accuracy was sufficient to observe differences in scale in the experiments.

3.2. *Penetration depth*

Penetration depth was measured in those targets that were not perforated. Since projectile erosion debris usually clogged the penetration channel, it was not possible to measure the actual depth of penetration directly. Instead, the last steel plate in the target was sectioned, and X-ray shadowgraphs developed. The difference between residual projectile and penetration channel were clearly distinguishable on the X-ray image. The depth of penetration was measured from the X-ray shadowgraph of each target.

3.3. *Projectile residual length and velocity*

X-ray shadowgraphs were taken at two times after perforation so that the residual velocity could be determined. The length of the rod after perforation was measured from these X-ray images. X-ray images of the residual rod and target debris on the exit side of a target from two tests (Test Nos. 8-0088 and 8-0090) are shown in Fig. 5. The impact velocities for the two tests were different, and the time delays for the flash X-rays were also different. Each picture is composed of three flash X-ray images. The first image shows the rear surface of the target plate, and the other two images are downrange from the target. In Fig. 5(a), the back of the target has just begun to bulge, so the projectile is approximately three to four projectile diameters away from the back surface of the target [1]. After perforation, the residual rod and target debris are clearly seen in the X-ray images. It is also evident in Fig. 5(a) that a portion of the front of the projectile—approximately one projectile diameter—has fractured and is separating from the main body of the residual rod. In Fig. 5(b), the X-ray image captured the breakout of the target. The debris bubble is approximately $3.5D$ long, and $4D$ wide at the time of the X-ray (the lateral extent of bulging of the back plate—also measured from the X-ray shadowgraph—is approximately $8D$ wide). This target must be perforated at the time of the flash X-ray (the maximum bulge height seen on perforated targets is approximately $2.0D$), but the target debris still obscures a view of the projectile. Because the impact velocity was

Fig. 5. Flash X-radiographs of breakout and residual projectile (1/3.15 scale): (a) Test 8-0088, $V_s = 2.18$ km/s, $V_r = 1.89$ km/s, (b) Test 8-0090, $V_s = 1.67$ km/s, $V_r = 1.14$ km/s.

less in Fig. 5(b) than Fig. 5(a) (1.67 km/s vs 2.18km/s), the residual rod in Fig. 5(b) is shorter than the rod in Fig. 5(a). The residual projectile, only a few diameters in length, is tumbling in Fig. 5(b).

3.4. *Hole diameter, crater height, bulge height, and interior damage diameter*

Entrance hole diameter, crater height on the target entrance side, and bulge height on the target exit side, were measured with vernier calipers. The entrance holes, for the very low yawed impacts, were essentially circular in shape. A number of measurements were averaged

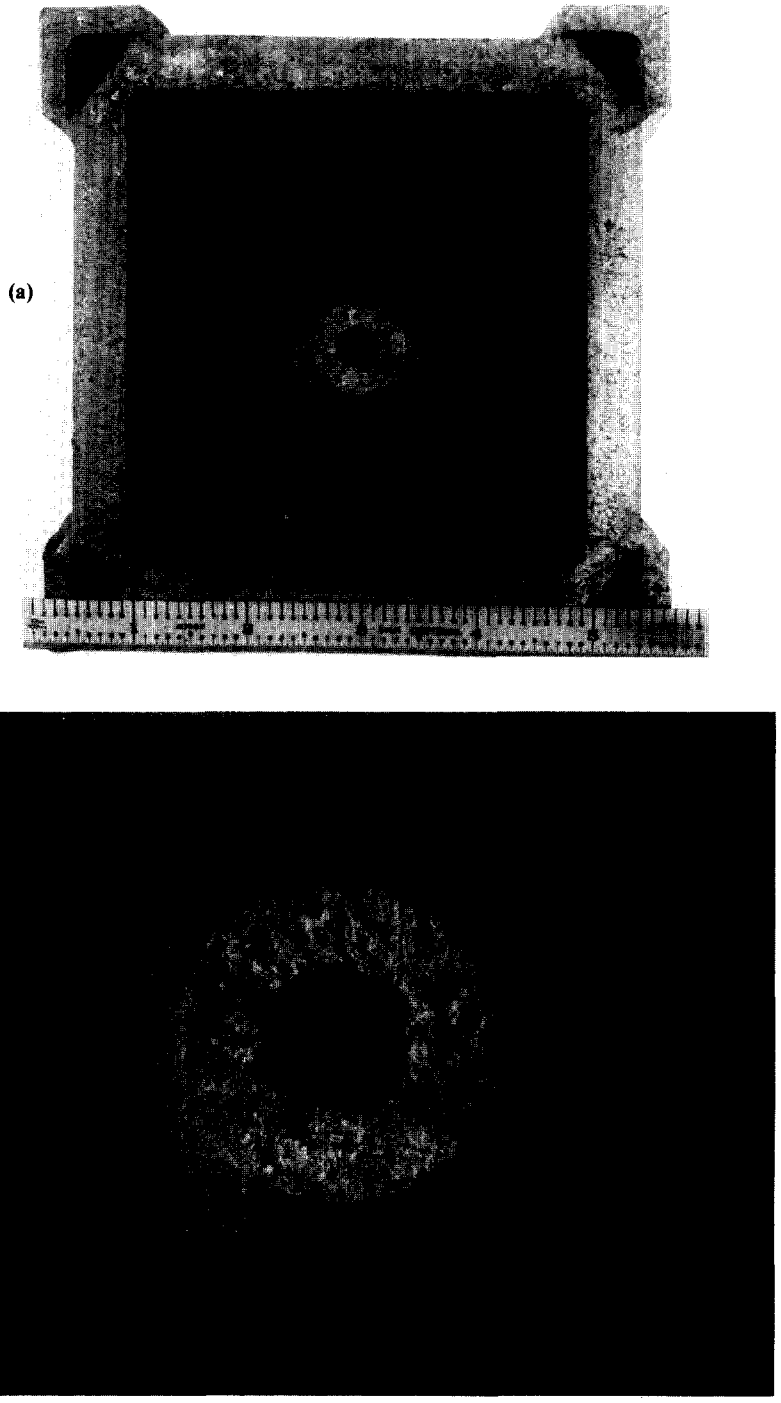

Fig. 6. Photograph of the damage feature measured from the interior of the first steel plate (Test 4-1492): (a) View inside the sectioned target, (b) Close-up view of the damage feature.

to determine the hole diameter given in Table 3. For cases where the projectile had significant inclination angle at impact, the entrance hole was elliptical. For these tests, both a maximum and minimum hole diameter were measured (see the top view of Fig. 4a), and both diameters are listed in Table 3. The entrance crater heights and exit bulge heights given in Table 3 are the maximum values measured. A damage feature was also measured on the interior side of the first steel plate. This interior damage has the appearance of a "flattened" bulge, apparently created when the first plate bulged in the direction of the flight path of the projectile; bulge growth is limited by the ceramic layer (a layer of "insulating" material separated the metal and ceramic elements). Figure 6 is a photograph of the interior damage feature (in this view, the projectile travelled towards the reader).

3.5. *Ballistic limit*

Several methods were used to determine the ballistic limit velocity. One of the preferred ways for determining V_{BL} is to fit the experimental data to the Lambert equation [6]:

$$V_r = \begin{cases} 0, & 0 \leqslant V_s \leqslant V_{BL} \\ a(V_s^p - V_{BL}^p)^{1/p}, & V_s > V_{BL} \end{cases} \tag{1}$$

where V_r, V_s, and V_{BL} are the residual, striking (impact), and limit velocities, respectively. The parameters found through a nonlinear regression fit to the experimental data are the slope a, the exponent p, and the limit velocity V_{BL}. The experimental data points, along with the results of the curve fits, are plotted in Figs 7 and 8 for the two target sets. Excessive projectile inclination at impact is denoted by an open symbol. The maximum velocity that could be achieved for the 1/3.15-scale projectile launch package was 2.33 km/s, and this velocity was not sufficient to perforate the thicker ($T/L = 1.378$) target. The ballistic limit velocities are given in Table 5 for cases where sufficient data existed to apply Eqn (1).

A second method to estimate the ballistic limit velocity examined the perforation (perf) vs no perforation (no perf) data as a function of impact velocity. In several cases, perforation occurred with only a small increase in impact velocity beyond a "no perf" datum, thereby providing a reasonably good estimate of the ballistic limit velocity. The estimates for the ballistic limit velocity using this procedure are also listed in Table 5.

The last procedure applied is the least precise of the three methods, but it permits an estimate for the limit velocity for targets not perforated and permits a correction to be approximated for impact inclination. For those projectiles that did not perforate the target, a velocity increment necessary to achieve perforation was estimated. We will refer to this

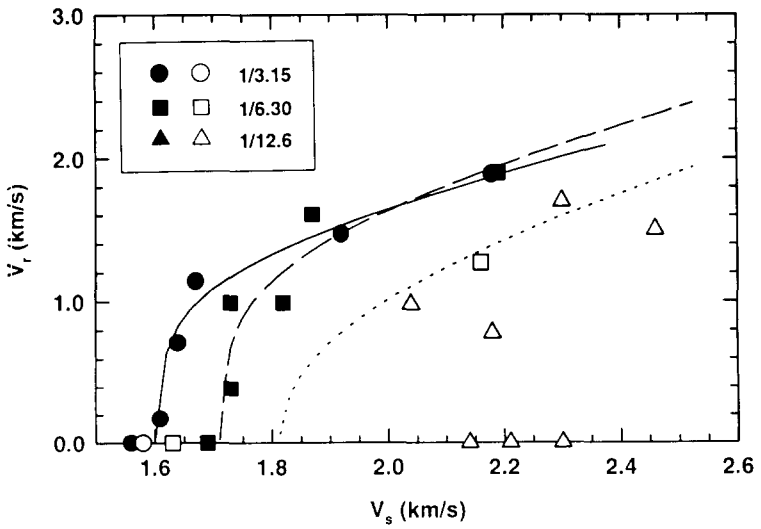

Fig. 7. Residual velocity vs impact velocity for $T/L = 0.945$ target. (Open symbols represent large impact inclination.)

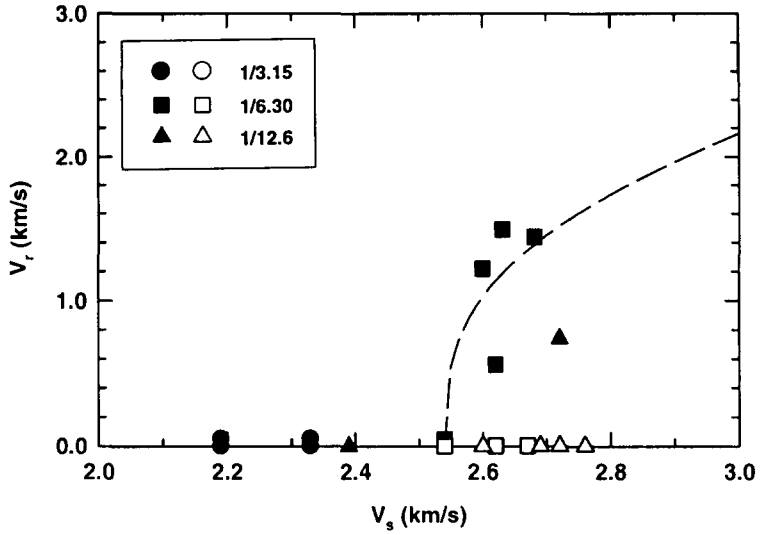

Fig. 8. Residual velocity vs impact velocity for $T/L = 1.378$ target. (Open symbols represent large impact inclination.)

Table 5. Estimates of ballistic limit velocities (km/s)

Scale size		$T/L = 0.945$			$T/L = 1.378$	
λ	Eqn (1)	Perf/no perf	$V + \Delta V$	Eqn (1)	Perf/no perf	$V + \Delta V$
1/3.15	1.61	1.59	1.65	–	>2.33	2.46
1/6.30	1.72	1.71	1.69	2.54	2.57	2.54
1/12.6	1.82	<2.04	<2.14	–	>2.39 <2.72	2.77

procedure as the $(V + \Delta V)$ method. The procedure makes use of the normalized penetration curve as a function of velocity. Figure 9 displays experimental data for $L/D = 20$ projectiles from a variety of sources [7–12].† The solid curve in the figure is a least-squares polynomial curve fit to the L/D 20 data:

$$\frac{P_\infty}{L} = -0.08516 + 1.135V_s - 3.890V_s^2 + 5.515V_s^3 - 3.274V_s^4 + 0.9598V_s^5 - 0.1385V_s^6 + 0.007872V_s^7, \quad (2)$$

and is valid for $0.50 \leqslant V_s \leqslant 4.5$ km/s. The regression correlation coefficient, r^2, is 0.993 for this curve fit. Clearly, there is no physical basis for the selection of a seventh-order polynomial; rather, it was selected to provide an analytical expression that faithfully reproduced the experimental data over the velocity range of interest. The derivative of Eqn (2) with respect to velocity gives the slope of the P_∞/L curve over the entire velocity range. An estimate of the velocity increment necessary to achieve an increment ΔP_∞ can be made from:

$$\Delta V = \frac{\Delta P_\infty / D}{(L/D)[\mathrm{d}(P_\infty/L)/\mathrm{d}V]}. \quad (3)$$

The increments of velocity necessary to achieve $\Delta P_\infty = D, 2D, 3D$ and $4D$ are shown in Fig. 10 as a function of impact velocity. It is seen that above 2.0 km/s, large increments of the impact

†To a first approximation, the projectile only "knows" that it is near the end of its penetration path, and the previous history (that it has penetrated a thick ceramic element) has been lost. Since the last element is steel, we feel justified in applying steel penetration data for $L/D = 20$ projectiles near the end of penetration.

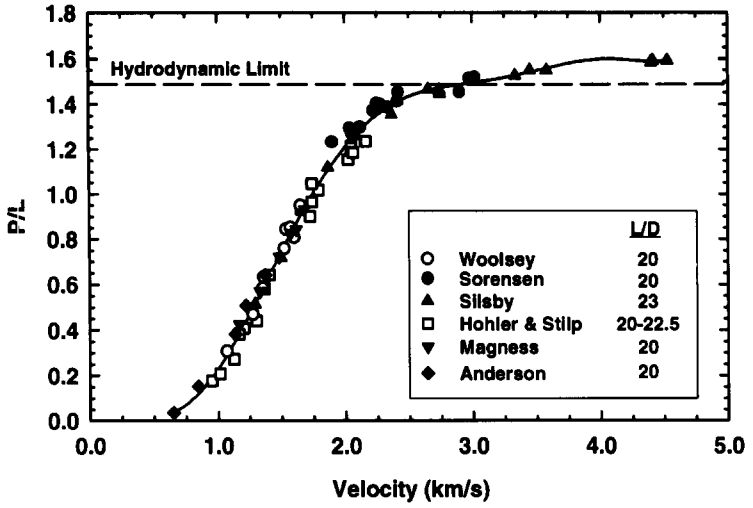

Fig. 9. Normalized penetration of semi-infinite targets vs impact velocity (Data from Refs [7–12].)

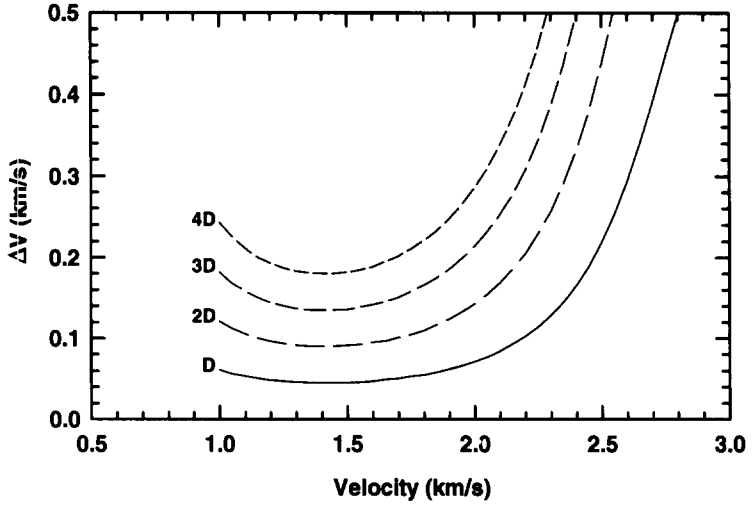

Fig. 10. Increment in impact velocity necessary for additional semi-infinite penetration.

velocity are required for small increments of penetration because of the flattening of the P_∞/L curve (Fig. 9) above 2.0 km/s.

Target bulging and failure create uncertainties in a methodology that is based on "semi-infinite" penetration. For the procedure here, we calculate the penetration (in projectile diameters) necessary to reach the original target back surface:

$$\frac{\Delta P_r}{D} = \frac{L}{D}\left(\frac{T}{L} - \frac{P_{exp}}{L}\right), \tag{4}$$

where P_{exp} is the experimentally determined depth of penetration into the target (from Table 3). To allow for less confinement in a finite target, the ΔV needed to achieve perforation is evaluated from Eqn (3) for $\Delta P_\infty/D \equiv (\Delta P_r - D)/D$.

Bjerke *et al.* [13], provide the basis for a first-order estimate of the effects of impact inclination (yaw). The critical yaw angle γ_{cr}, the angle at which the tail of the projectile just strikes the entrance hole, is defined by the expression:

$$\gamma_{cr} = \sin^{-1}\left[\frac{H/D - 1}{2(L/D)}\right]. \tag{5}$$

The derivation of Eqn (5) assumes that the yaw does not change during the penetration event. The normalized hole diameter H/D as a function of impact velocity (discussed further in the next section) was determined by combining all the data into a single data set and performing a linear least-squares regression fit:

$$\frac{H}{D} = 0.37 + 0.84V_s. \tag{6}$$

An empirical equation that appears to describe the degradation of experimentally measured P/L as a function of impact yaw is given by [13]:

$$\left(\frac{P_{\text{degrade}}}{L}\right) = \left(\frac{P_\infty}{L}\right)\cos(11.46\gamma_{cr}/\gamma). \tag{7}$$

In the experiments, the degraded value of P/L is measured, so we use Eqn (7) to estimate (P_∞/L) to use for (P_{exp}/L) in Eqn (4). Our experience is that penetration performance is barely affected, if at all (within experimental scatter), for impact yaws up to 1.5–2.0 times γ_{cr}; therefore, Eqn (7) is applied only to data where the total yaw was greater than $2\gamma_{cr}$.

The $V + \Delta V$ method was applied to both target sets. The method gives reasonable answers (within 0.05 km/s) for V_{BL} for the cases where Eqn (1) and the perf/no perf methods could be applied; see Table 5. For the 1/3.15-scale and the 1/12.6-scale tests, for which $T/L = 1.378$, the $V + \Delta V$ method provided the only estimate for V_{BL} (although the perf/no perf procedure was used to place constraints on acceptable values). As already noted, the 1/12.6-scale experiments were plagued by excessive yaw, and impact inclination generally increased as the impact velocity was increased.

We now want to place uncertainties on the estimates for the ballistic limit velocities. Methodologies have been developed to permit estimates of the ballistic limit velocity from a relatively small number of tests [14]. Central to these methodologies is the recognition that over a specified velocity range, either a partial or a complete penetration of a target may occur— a zone of mixed results—with the percentage of complete penetrations over this range increasing as the impact velocity increases. Experience has shown that the zone of mixed results is 0.020–0.050 km/s wide for metallic armor materials. That is, the ballistic limit velocity is ± 0.010 to ± 0.025 km/s about some mean velocity, usually referred to as V_{50}, which for purposes here is considered to be synonymous with V_{BL}. For example, in Ref. [15], the ballistic limit velocities were determined for two different target thicknesses within ± 0.010 km/s with a very small number of tests.

With the preceding paragraph as background, the results of Table 5, plus a review of all the data, were used to arrive at our best estimate of the ballistic limit velocities and the associated uncertainties, Table 6. Typically, for cases where perf/no perf data exist, the limit velocity is taken to be the average of the two impact velocities, and the uncertainty is the distance between this average and either data point. To be conservative, we have doubled this uncertainty. A similar analysis has been applied to the data in Table 5, subject to the constraints imposed by "perf/no perf". The uncertainties in Table 6 reflect at least, we believe, a 2σ value for V_{BL}.

3.6. *Target design*

Targets were "tougher" to penetrate than originally expected. The targets were designed using experimental data for $L/D = 10$ projectiles. It has been shown that there exists

Table 6. Ballistic limit velocities and uncertainties (km/s)

Scale size λ	$T/L = 0.945$	$T/L = 1.378$
1/3.15	1.60 ± 0.04	2.40 ± 0.10
1/6.30	1.71 ± 0.04	2.55 ± 0.04
1/12.6	1.90 ± 0.16	$2.70^{+0.04}_{-0.10}$

	Scale	T/L
○	1/3.15	0.945
●	1/3.15	1.378
□	1/6.30	0.945
■	1/6.30	1.378
△	1/12.6	0.945
▲	1/12.6	1.378

Fig. 11. Legend for Figs 12–16.

a significant L/D effect for projectiles with aspect ratios greater than 10 [16–18]. Penetration performance in the ordnance velocity range is degraded approximately 14% as the projectile L/D increases from 10 to 20. This translates into a higher impact velocity for perforation if the L/D of the projectile is increased for constant T/L, since the larger L/D projectiles are less efficient in penetration. We note here that the thicker of the two targets ($T/L = 1.378$) almost represents the maximum thickness that can be perforated by the projectiles used in this study.

4. ANALYSIS OF SCALING EFFECTS

Analysis of the experimental data seeks to determine whether there is a systematic difference in response as a function of scale, beyond that attributable to measurement uncertainty. It is possible that scale effects may be apparent in some response measurements, but not others. Each subsequent section discusses the ballistic response variables measured in the ballistic experiments. Figure 11 provides the legend for the remainder of the figures in the paper.

A factor that complicated the scaling analysis was total yaw (inclination) of the rod at impact. As might be expected, tests with considerable impact inclination display different results than otherwise identical tests with low yaw. Where possible, comparisons of the response data were conducted for low inclination data. For penetration, a "correction" for inclination was applied in an attempt to make use of all data. Since there exists little formal documentation of the effects of yaw, some of the response data in this section are plotted as a function of yaw.

4.1. *Hole size, crater height, and interior damage diameter*

Although maximum and minimum entrance hole diameters were measured for each target, minimum hole diameter was used in the scaling comparisons because it tended to be independent of total yaw, making more data available for comparisons. The entrance hole diameter and crater height are combined for both scaled target thicknesses since they do not depend upon target extent, i.e. these features are frontal surface effects and should not be affected by target thickness (for targets more than several projectile diameters thick).

Figure 12 shows nondimensional minimum hole diameter (H_{min}/D) as a function of total yaw for all the targets. These data are plotted vs impact velocity in Fig. 13. Likewise, the nondimensional crater heights (C/D) are plotted in Figs 12 and 13. It should be noted that in many of the experiments, the pusher plate hit the target front face and prevented any measurement of the hole diameter and crater height (see Table 3). The nondimensional interior damage diameters (D_i/D) vs total yaw and impact velocity are also plotted in Figs 12 and 13. Although D_i/D is not a surface feature, the response occurs sufficiently early in the penetration history that it should be insensitive to total target thickness.

Figure 12 demonstrates the relative independence of nondimensional hole diameter upon total yaw. There is some appearance of a scale size effect (the 1/3-scale data lie below the 1/6-scale data), but this is due primarily to different impact velocities for the various scale sizes, as shown by Fig. 13. The C/D and D_i/D data demonstrate a similar relative independence upon total yaw up to about 8°. Beyond 8°, there may be a yaw dependence, although the paucity of data precludes any firm conclusions. Again, the appearance of a scale size effect for C/D and D_i/D in Fig. 12 is really a velocity effect, as shown by Fig. 13.

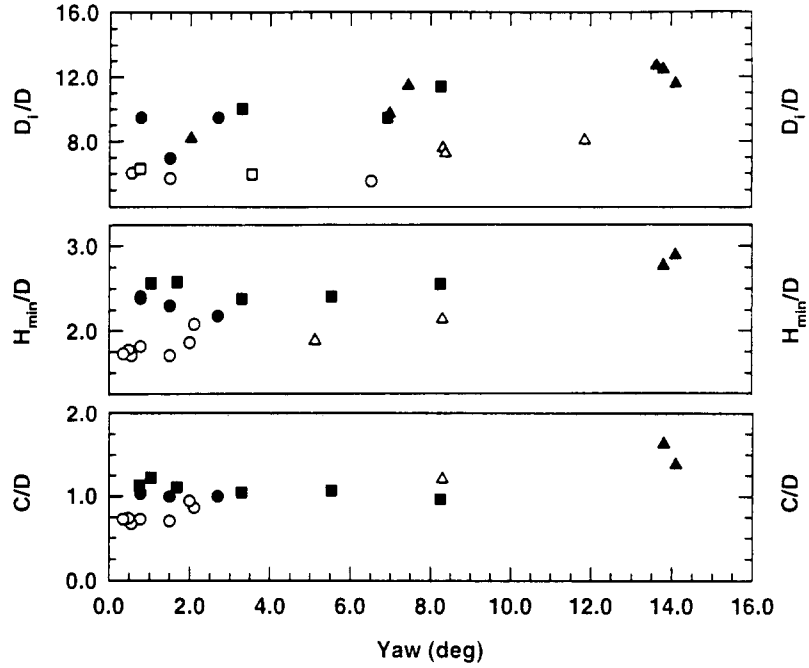

Fig. 12. Nondimensionalized response variables as a function of impact yaw.

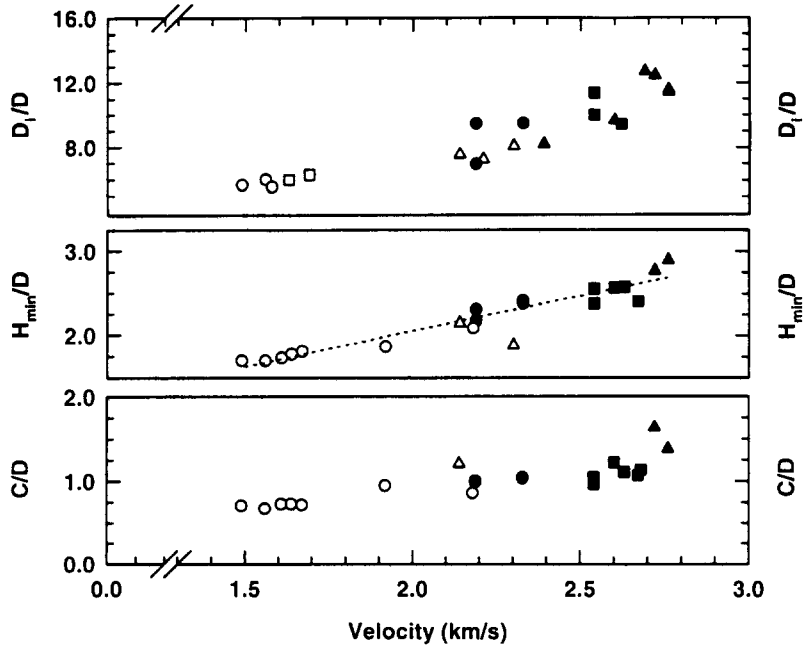

Fig. 13. Nondimensionalized response variables as a function of impact velocity.

It is difficult to do one-to-one comparisons for the different scale sizes because there is little overlap in impact velocity.† In Fig. 13, it can be seen that the data for all three scale sizes tend to indicate a single relationship for hole size as a function of velocity [Eqn (6)]. That is, there does not seem to be any indication of different slopes or offset due to scale size. This effect is also visible for C/D and D_i/D. No scale size effect is apparent in the data. However, it may be

†It should be remembered that the objective of the experiments was to determine V_{BL}, not to have direct comparison between scales at the same impact velocity. Nevertheless, we have critically examined the data to make comparisons and draw conclusions where we can.

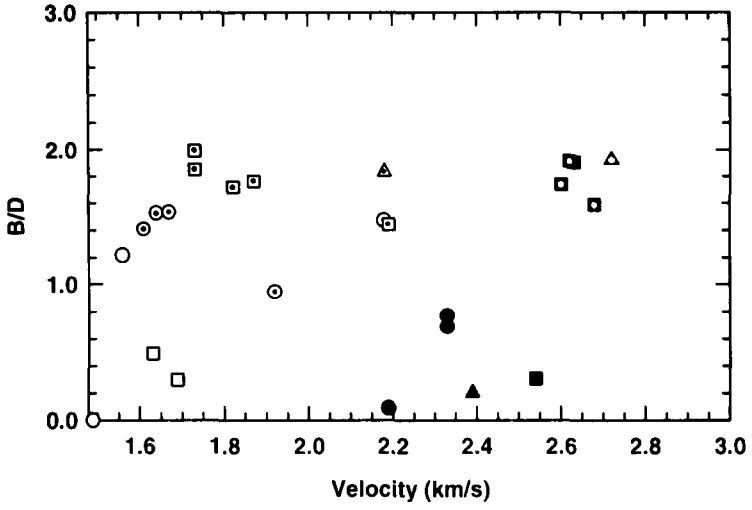

Fig. 14. Nondimensional bulge height vs impact velocity. (Dot in center of symbol represents a perforated target.)

misleading to conclude that there are no scale size effects for these three response variables since virtually no data at the same impact velocity with low yaw exist for a comparison. In Ref. [5], normalized entrance hole diameter and crater height increased approximately 6% as the scale changed from 1/12 to 1/3 at 1.5 km/s for 0° obliquity targets; whereas, no scale effect was evident at 2.2 km/s. Strong scaling effects at both impact velocities were observed on the normalized crater height for 60° obliquity targets.

4.2. *Bulge height*

Figure 14 shows B/D as a function of impact velocity for both of the scaled target thicknesses (only data with yaws less than 3.6° are plotted). The data fall into two groupings: perforated targets (dot in the middle of the symbol), and nonperforated targets. When a target is perforated, the bulge is a measure of the height of the exit hole uplift region. When not perforated, the bulge is a measure of the strain in the last element of the target.

For the perforated targets, the extent of bulging is approximately 1.2–1.9 projectile diameters, and it appears to be relatively independent of velocity (for the velocity range investigated). When a target is perforated, the breakout of the projectile pushes target material outwards; thus, the height of the bulge increases with target perforation. B/D for the 1/3-scale targets clearly lie below the other two scales. (Although there appears to be a tendency for the 1/6-scale data to lie below the 1/12-scale data, their exists only two 1/12-scale data points.) We believe the primary reason B/D for the 1/3-scale targets are smaller than the other two scales is that the 1/3-scale targets have a scab ring surrounding the exit hole; the other two scales do not exhibit this behavior. The rear surface of perforated targets exhibit more fracture damage at 1/3 scale.

Examination of the data suggests that the maximum bulging of the rear surface of the steel target, before perforation, is approximately 1.2 projectile diameters. In Fig. 14, it is possible to see some indication of a scale size effect for the nonperforation data. For the $T/L = 1.378$ target set, the 1/3-scale data have a larger average B/D than the 1/6-scale point, which is, in turn, larger than the 1/12-scale point. This trend occurs even though the velocity was higher for the 1/6- and 1/12-scale tests as compared to the 1/3-scale tests. A similar trend is observed for the $T/L = 0.945$ target set when comparing the 1/3- and 1/6-scale data.

4.3. *Penetration depth*

Nondimensional penetration depths P/L are plotted in Fig. 15 for the targets that were not perforated. Two of the 1/12-scale and two of the 1/6-scale data points in Fig. 15 were high yaw

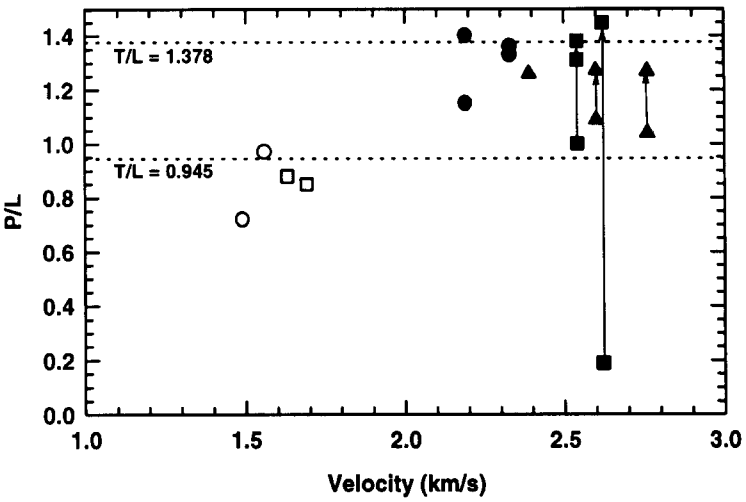

Fig. 15. Nondimensional penetration depth for targets not perforated.

shots that were "corrected," per the method described in Section 3.5; the arrows denote the change in the penetration depth after the correction was applied.

Although there are only a few data points available for comparison, Fig. 15 demonstrates that the average penetration depth increases as scale size increases. The average P/L value for the 1/6-scale targets is larger than the average of the 1/12-scale values, even though the impact velocities are higher for the 1/12-scale tests. Similarly, the average 1/3-scale P/L value is about equal to the average 1/6-scale value, but the impact velocities for the 1/3-scale tests were less. Although the paucity of data prevents quantifiable measures of the scale size effect, a trend of "tougher" targets as scale size decreases is demonstrated.

4.4. *Residual projectile length and velocity*

Table 7 lists selected projectile residual length and residual velocity data that can be compared directly due to similar impact velocities. All data have total yaw less than 3.6°, and have been separated by target thickness.

For the thicker targets ($T/L = 1.378$), comparisons can be made only for the 1/6- and 1/12-scale sizes because there were no perforations of the 1/3-scale targets. Comparing the 2.72-km/s, 1/12-scale test to the four 1/6-scale tests that range in velocity from 2.60 to 2.68 km/s, it can be seen that the 1/12-scaled data are smaller. The normalized residual velocity is less, as is the normalized residual length (the 1/12-scale residual length is a "thin" fragment, the smallest size that can be determined).

For the thinner targets ($T/L = 0.945$), the impact velocity of approximately 2.20 km/s can be investigated. The data indicate that the 1/12-scale residual velocity and length are less than

Table 7. Limited comparisons of residual projectile velocity and length

Scale size λ	V_s (km/s)	$T/L = 0.945$ V_r/V_s	L_r/D	$T/L = 1.378$ V_r/V_s	L_r^2/D
1/3.15	2.18	0.87	4.16		
1/6.30	2.68			0.54	0.50
	2.63			0.57	0.76
	2.62			0.21	frag
	2.60			0.47	0.76
	2.19	0.87	4.35		
1/12.6	2.72			0.27	frag
	2.18	0.36	frag		

the comparable 1/6-scale data. However, there does not appear to be a difference between the 1/6- and 1/3-scale data.

Although the comparisons are extremely limited, these data tend to indicate that the 1/12-scale targets are harder to perforate than 1/3- and 1/6-scale targets.

4.5. *Ballistic limit velocity*

A large body of evidence exists for a fundamental energy scaling principle in which some critical energy is a constant [19]:

$$E_c = \text{constant}, \tag{8}$$

where E_c has units of energy per unit area. Examples include detonation of explosives, spall strength, failure of brittle structures, aspects of shear banding, and fragmentation [20–23]. For the case here, we write Eqn (8) in the form:

$$\rho_p V_{BL}^2 l = \text{constant}, \tag{9}$$

where l is some characteristic length, such as projectile length or target thickness. Length scales as the geometric scale factor λ, which then suggests

$$V_{BL} \propto \lambda^{-1/2}. \tag{10}$$

The ballistic limit velocities with their uncertainties are plotted vs the inverse square root of the scale size in Fig. 16. Over a scale factor of four, the observed differences between the ballistic limit velocities are greater than the uncertainties in the determination of V_{BL}. The results of Fig. 16 indicate that V_{BL} increases as the scale size decreases, and that V_{BL} is approximately linear with respect to $\lambda^{-1/2}$.

A linear least-squares regression fit was performed as a function of $\lambda^{-1/2}$. Data points were weighted by the inverse of their uncertainty prior to the regression analysis. Results of the regression analyses are, with V_{BL} in km/s:

$$V_{BL} = 1.30 + 0.165\lambda^{-1/2} \quad T/L = 0.945 \quad (r^2 = 0.995) \tag{11a}$$

$$V_{BL} = 2.12 + 0.166\lambda^{-1/2} \quad T/L = 1.378 \quad (r^2 = 0.983). \tag{11b}$$

The linear least-squares fits to the data are shown as the dotted lines in Fig. 16. Note that the slopes in Eqns (11) are independent of T/L. Of course, Eqns (11) apply **only** to the materials and geometries, i.e. projectile and target configuration, tested.

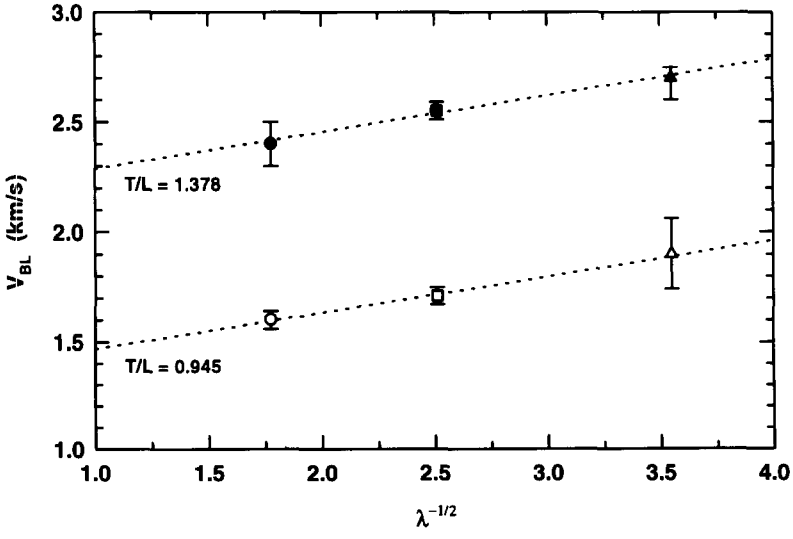

Fig. 16. Ballistic limit velocities vs scale size.

It is possible to extrapolate the subscale data to full scale to estimate the ballistic limit velocity at full scale. Setting $\lambda = 1$ in Eqns (11) gives 1.46 km/s and 2.29 km/s for the two target thicknesses, respectively; thus, V_{BL} for full scale is significantly lower than would be predicted by each subscale test. These targets have not been built or tested at full scale, so we do not have confirmation of the full-scale prediction. However, it appears that the apocryphal stories are true that subscale results are different than full-scale results in armor penetration experiments. In fact, the results here show that subscale tests will overestimate the effectiveness of an armor system.

5. SUMMARY AND DISCUSSION

A series of tests at three scale sizes was performed to determine the ballistic limit velocities of two ceramic laminate targets; the second target was 50% thicker than the first and therefore required higher impact velocities for perforation. Other measures of ballistic performance were recorded in addition to the ballistic limit. Ballistic response measurements taken from the first steel plate of the target—the entrance hole diameter, the entrance hole crater height, and the bulging of the back surface of the first steel plate (the so-called interior damage diameter)—did not demonstrate a scale size effect, although the data that could be compared directly (identical impact velocities) at different scales were insufficient to conclude that scale effects do not exist. However, a dependency of these responses on impact velocity was observed.

Other ballistic response measures tended to indicate a scale-size effect; however, because of the small quantity of comparable data, the effect could not be quantified. These measurements included penetration depth in targets not perforated, residual projectile length and velocity for perforated targets, and the bulge height on the target rear plate. For all of these measures, target resistance to penetration appeared to increase as the scale size became smaller. For example, 1/12-scale targets had lower normalized residual velocity, less penetration depth, and lower bulge height than comparable 1/13-scale targets tested at approximately the same impact velocity.

The scale size effect could be quantified for the ballistic limit velocity since the test series was specifically designed to determine this response parameter. (Parenthetically, we note that the scale size dependency of the response variables described in the previous paragraph are consistent with a ballistic limit velocity scale effect). It was found that V_{BL} decreased with increasing scale size. For the two ceramic laminate targets tested in this study, V_{BL} changed by approximately 120 m/s for a factor of two change in the scale size [Eqn (11)]. Since the scale sizes were varied over a factor of four, a reasonable extrapolation can be made to estimate full-scale response. For example, for the impact conditions and types of targets and projectiles tested here, this study indicates that 1/6-scale targets could overpredict full-scale response by approximately 15%.

What is the underlying cause of the scale effect? It was demonstrated in Ref. [1], using numerical simulations, that strain-rate hardening cannot be used to explain differences of more than 5% over a scale factor of 10. Lending support to the computational study is an experimental investigation by Wen and Jones [2] where they found geometrically similar responses over a scale factor of four, even when using strain-rate sensitive materials (albeit the experiments were performed at a considerably lower impact velocity).

It was suggested in Ref. [1] that a possible explanation for the scale size effect is the difference in absolute time available for damage or failure to evolve. Failure of the target and projectile depend upon the stress state and accumulation of damage. The stress state at the various scales is very nearly the same, since the stresses are primarily a function of impact velocity (with only a little dependence on strain rate). On the other hand, damage accumulates with time. In these scale model experiments, time scales as λ, which means that events happen faster in the subscale models (for example, time is reduced by a factor of four in going from the 1/3-scale tests to the 1/12-scale tests).

If differences in damage evolution are to be a plausible explanation of the scaling effect, it must be demonstrated that the characteristic failure times are approximately the same as the

loading times. We offer the following example. It is observed experimentally that the spall strength of metals, e.g. Armco iron and 6061-T6 aluminum, decreases by a factor of two as the pulse width changes from 0.05–0.10 μs to 0.30–0.40 μs, which implies that a characteristic damage time for spallation (a wave propagation phenomenon) is of the order of several tenths of a microsecond [24]. The failure mode of the targets in the present work is not spallation, but order-of-magnitude estimates can be made of the failure time for the experiments reported here. It might be expected, for ballistic experiments, where the operative mechanism is large-field plastic flow, that characteristic damage times might be an order of magnitude longer than for spallation, i.e. of the order of a few microseconds. An estimate of the loading time is obtained from nominal steady-state penetration. For the order-of-magnitude estimates here, the erosion rate of the projectile is approximately one-half the impact velocity, e.g. 1.0 km/s. Since the projectile opens a cavity approximately 2.0 projectile diameters, a characteristic loading time is estimated to be of the order of 2–8 μs as the scale factor changes from 1/12 to 1/3. Clearly, these order-of-magnitude estimates are heuristic, but it appears plausible that characteristic loading and failure times are similar.

Therefore, we postulate that the root cause of the differences in ballistic response as a function of scale size is due to differences in damage history and failure. For example, we noted that the 1/3-scale targets had a scab ring surrounding the exit hole; such a feature was not observed at the other scales. Another example concerns the "interior damage ring" that is shown in Fig. 6. Full-scale tests of a proprietary target have been performed where an isolation material (analogous to the Fiberfrax used in the tests reported here) was placed between the steel and the ceramic. The same damage feature shown in Fig. 6 was observed, but in the full-scale tests, this feature exhibits considerably more damage (not just bulging). In some of the full-scale tests, this ring actually scabbed, having the appearance of a spall ring [25]. In the experimental study of Ref. [5], considerably more damage (tearing and scabbing) is observed around entrance and exit holes at the 1/3.15-scale size than for the smaller scales, particularly for the oblique targets.

Atkins postulated, for situations in which extensive plastic flow precedes and accompanies fracture, that geometric nonscaling is a consequence of work done in opening and driving cracks [3]. He examined very low velocity impact problems and demonstrated experimental support for his postulate. Even if Atkins' work is extended to include other failure mechanisms (e.g., ductile void growth and coalescence, and shear localization), there are essential differences between Atkins' explanation and the one given here. For ballistic problems, the energy dissipated in plastic work dominates the mechanics; energy losses in fracture are very small relative to the plastic work, and therefore, geometric scaling should be satisfied within experimental variability (in low velocity impacts, energy absorbed in fracture processes is significant relative to energy dissipated in plastic flow, as Atkins has demonstrated). In Atkins nomenclature, the nondimensional variable ξ, which is essentially a measure of the ratio of energy dissipated in plastic work to that dissipated in fracture, is large for ballistic impact problems; therefore, geometric scaling distortion cannot be determined from the energy arguments of Atkins. Instead, it is the details of damage evolution that are important because damage scales as absolute time instead of scaled time; thus, small targets do not have the same amount of "damage" at homologous times. This is particularly important near a threshold condition such as the ballistic limit. The next paragraph describes one way in which the two postulates can be differentiated.

Further study is warranted where the focus is investigation and understanding of the origins of the scale effect. An ancillary question is whether it is the failure of target material or projectile material, or both, that needs to be invoked to account for the experimentally observed differences. Another relevant question is whether the scale effect saturates at some point. Equations (11) were extrapolated to full scale by setting λ equal to 1.0. But at some point, assuming that the scale effect is caused by a damage rate effect, the absolute times will be sufficiently long that damage will saturate. Therefore, further increases in scale size will not result in more damage; experimental results should then be independent of scale size. Where the scale effect saturates, if it does, remains to be determined, and is also an open research question.

Acknowledgements—This work was performed under contract DAAL03-91-C-0021 with the U.S. Army Research Office. A number of people at SwRI provided considerable assistance in various aspects of this research effort. Mr. Bruce Morris was responsible for the design and fabrication of the targets. Ms. Suzanne Royal assisted in data reduction. The authors would like to acknowledge the support and encouragement of Dr. Thomas Kiehne, formerly of the Defense Advanced Research Projects Agency, and now at the Institute for Advanced Technology, Mr. Billy Hogan of Los Alamos National Laboratory, and Mr. René Larriva of Interferometrics. Lastly, the authors would like to acknowledge the contribution of Dr. Dennis Grady, of Sandia National Laboratories, who provided the key suggestion for plotting the ballistic limit velocity as the inverse square root of the scale size, and pointing out other examples of the energy scaling relationship.

REFERENCES

1. C. E. Anderson, Jr., S. A. Mullin and C. J. Kuhlman, Computer simulation of strain-rate effects in replica scale model penetration experiments. *Int. J. Impact Engng* **13**(1), 35–52 (1993).
2. H.-M. Wen and N. Jones, Experimental investigation of the scaling laws for metal plates struck by large masses. *Int. J. Impact Engng* **13**(3), 485–505 (1993).
3. A. G. Atkins, Scaling in combined plastic flow and fracture. *Int. J. Mech. Sci.* **30**(3/4), 173–191 (1988).
4. L. Magness, Jr. and W. Leonard, Scaling issues for kinetic energy penetrators. *Proc. 14th Int. Symp. on Ballistics*, Vol. 2, pp. 281–289, Québec City, 26–29 September (1993).
5. S. A. Mullin, C. E. Anderson, Jr., N. W. Blaylock, B. L. Morris, Jr., A. J. Piekutowski and K. L. Poormon, Scale model penetration experiments: finite-thickness steel targets. SwRI Report 3593/003, Southwest Research Institute, San Antonio, TX (1995).
6. J. A. Zukas, T. Nicholas, H. G. Swift, L. B. Greszczuk and D. R. Curran, *Impact Dynamics*, Chapter 5. John Wiley, New York (1982).
7. P. Woolsey, in *A Penetration Mechanics Database* (Edited by C. E. Anderson, Jr., B. L. Morris and D. L. Littlefield). SwRI Report 3593/001, Southwest Research Institute, San Antonio, TX (1992).
8. B. R. Sorensen, K. D. Kimsey, G. F. Silsby, D. R. Scheffler, T. M. Sherrick and W. S. deRosset, High velocity penetration of steel targets. *Int. J. Impact Engng* **11**(1), 107–119 (1990).
9. G. F. Silsby, Penetration of semi-infinite steel targets by tungsten long rods at 1.3 to 4.5 km/s. *Proc. 8th Int. Symp. on Ballistics*, Orlando, FL, 23–25 October (1984).
10. V. Hohler and A. J. Stilp, in *A Penetration Mechanics Database* (Edited by C. E. Anderson, Jr., B. L. Morris and D. L. Littlefield). SwRI Report 3593/001, Southwest Research Institute, San Antonio, TX (1992).
11. L. S. Magness and T. G. Farrand, Deformation behavior and its relationship to the penetration performance of high-density KE penetrator materials. *1990 Army Science Conference*, Durham, NC (1990).
12. C. E. Anderson, Jr., unpublished data.
13. T. W. Bjerke, G. F. Silsby, D. R. Scheffler and R. M. Mudd, Yawed long-rod armor penetration. *Int. J. Impact Engng.* **12**(2), 281–292 (1992).
14. ——— Elements of terminal ballistics, Part 2, Collection and analysis of data concerning targets. AMCP 706-161, Army Material Command Engineering Design Handbook Series, U. S. Army Material Command (1962).
15. C. E. Anderson, Jr., V. Hohler, J. D. Walker and A. J. Stilp, Time-resolved penetration of long rods into steel targets. *Int. J. Impact Engng* **16**(1), 1–18 (1995).
16. Y. Partom and D. Yaziv, Penetration of L/D = 10 and 20 tungsten alloy projectiles into RHA. In *High Pressure Science & Technology—1993*, Vol. 2, pp. 1801–1804 (Edited by S. C. Schmidt, J. W. Shaner, G. A. Samara and M. Ross). AIP Press, NY (1994).
17. Z. Rosenberg and E. Dekel, The relation between the penetration capability of long rods and their length to diameter ratio. *Int. J. Impact Engng* **15**(2), 125–129 (1994).
18. C. E. Anderson, Jr., J. D. Walker, S. J. Bless and Y. Partom. On the *L/D* effect for long-rod penetrators. *Int. J. Impact Engng* **18**(3) (1996). To be published.
19. D. E. Grady, Sandia National Laboratories, private communication (1994).
20. W. E. Baker, M. G. Whitney and V. B. Parr, Scaling of initiation of explosives by fragment impact. *Shock and Vibration Bulletin* **50**, 199–211 (1980).
21. B. H. Bergstrom, C. L. Sollenberger and W. Mitchell, Jr., Energy aspects of single particle crushing. *Trans AIME* **220**, 367–372 (1961).
22. A. G. Ivanov and V. N. Mineev, Scale effects in fracture. *Combust. Explo. Shock Waves* **15**(5), 617–638 (1979).
23. D. E. Grady and J. Lipkin, Criteria for impulsive rock fracture. *Geophysical Research Letters* **7**(4), 255–258 (1980).
24. L. Davison and R. A. Graham, Shock compression of solids. *Physics Reports* (Review section of *Physics Letters*) **55**(4), 255–379 (1979).
25. W. Gooch, Army Research Laboratory, private communication (1994).